EUROPHYSICS LETTERS 1 December 1992

Europhys. Lett., 20 (7), pp. 645-650 (1992)

Scanning Hall-Probe Microscopy of a Vortex and Field Fluctuations in $La_{1.85}Sr_{0.15}CuO_4$ Films.

A. M. CHANG(*), H. D. HALLEN(*), H. F. HESS(*), H. L. KAO(**)(§), J. KWO(*) A. SUDBØ(*) and T. Y. CHANG(***)

(*) *AT&T Bell Laboratories - Murray Hill, NJ 07974-0636*
(**) *Department of Electrical Engineering, Columbia University - New York, NY 10027*
(***) *AT&T Bell Laboratories - Holmdel, NJ 07733*

(received 16 July 1992; accepted in final form 21 September 1992)

PACS. 74.30C – Magnetization curves, Meissner effect, penetration depth.
PACS. 74.60G – Flux pinning, flux motion, fluxon-defect interactions.
PACS. 61.16 – Other determination of structures.

Abstract. – A high-resolution scanning Hall-probe microscope is used to spatially resolve vortices in high-temperature superconducting $La_{1.85}Sr_{0.15}CuO_4$ films. At low magnetic fields, a disordered vortex arrangement is observed. A fit to the surface field of an individual vortex is consistent with one flux quantum, and is used to determine the local penetration depth and its temperature dependence. At higher fields, magnetic fluctuations are observed and compared to a collective pinning model. For films grown with the *c*-axis tilted from the surface normal, oval vortices are observed.

A detailed understanding of the magnetic fields in a superconductor is central to much of our understanding of this remarkable phase of matter. Knowledge of the spatial field fluctuations determines both the magnetic penetration depth, which defines the size of a vortex, and also the positions and ordering of the flux lines. In this letter we address both aspects through *local, quantitative,* and high spatial resolution ($\sim 0.3\ \mu m$) measurements of the field just above the surface of a superconductor using a new implementation of the scanning Hall-probe microscope [1] (1).

Initially we will demonstrate how vortices can be imaged and the field profile of an *individual* vortex can be analyzed to extract the local penetration depth in a high-temperature superconductor. This is direct and very local, in contrast to the more traditional methods of penetration depth measurement such as μSR [3], NMR [4], or neutron diffraction [5] that evaluate the averaged field distributions using assumptions of a (possibly

---

(§) Present address: Materials Research Center, Hsing-hua University, Hsin-chu, Taiwan.

(1) In a previous study Itzler *et al.* [2] employed a similarly fabricated Hall probe, but without as fine positioning and scanning capabilities.

imperfect) vortex lattice and a homogeneous sample to determine the penetration depth.

Finally we address the issue of vortex ordering in superconductors [6-11], which has recently generated considerable interest. Traditionally Bitter patterns [8, 9] and neutron diffraction [6], more recently electron holography [10] and potentially magnetic force microscopy [11] can be used to identify vortex locations. Unlike the first and last method one would prefer a nondestructive and nonperturbative imaging method so that the same local region can be studied at different fields and temperatures. Further, one desires a method which can be used on a variety of sample types: bulk samples, small samples and thin films. At low fields the scanning Hall-probe microscope can identify individual-vortex locations in such a manner. At much higher fields, which are necessary for comparison with interacting-vortex theory for strongly pinning samples, the Hall-probe microscope provides a quantitative measure of spatial vortex density fluctuations—a feat which is beyond the capabilities of the other techniques.

Our scanning Hall-probe microscope provides a direct measurement of the normal component of the magnetic field at close proximity to the surface of a sample. The apparatus consists of a submicron Hall bar patterned within 3.5 μm of one corner of a $GaAs/Al_{0.3}Ga_{0.7}As$ heterostructure chip. It has a field resolution of ~ 0.2 G at a 1 s time constant under optimal operating conditions of low temperatures ($T \sim 4.2$ K) and a spatial resolution of ~ 0.35 μm. The fabrication of the Hall probe employs electron-beam lithography, photolithography, and shallow etching techniques [12]. The chip is mounted onto a low-temperature scanning tunneling microscope stage. The distance of the probe above the surface can be accurately determined by briefly establishing a tunneling contact. A more detailed description of the fabrication process and experimental technique will be provided elsewhere [13].

Two $La_{1.85}Sr_{0.15}CuO_4$ films were prepared by *in situ* growth using a 90° off-axis sputtering under conditions previously described [14]. The (001) oriented film 0.8 μm thick was grown on a (100) $SrTiO_3$ substrate, and the (103) oriented film 0.55 μm thick was grown on a vicinal (101) $SrTiO_3$ substrate yielding a single-domain film with the CuO_2 planes uniaxially tilted off the substrate by 49° [15]. The resistive $T_c(R = 0)$ is 28.0 K, and 35.0 K for (001) and (103) films, respectively.

As the Hall bar sweeps, it makes a map of the magnetic field in the direction normal to the surface (z-direction). Two such maps are shown in fig. 1. These are images taken 0.21 μm above the surface of the (001) film after cooling in a 5 G field oriented perpendicular to the surface. They show several similar circular features up to ~ 7 G in field amplitude and ~ 0.8 μm in diameter. An integration of the measured field in an area ~ 8 μm^2 about a feature yields a flux $\sim (0.8 \div 0.9)$ of a flux quantum $\Phi_0 = hc/2e'$ consistent with a vortex quantized at Φ_0. The remaining $\sim (0.1 \div 0.2)$ Φ_0 passes the plane of the scan beyond the boundary of the integration range. We thus identify these features as individual quantized vortices. They do not form a regular lattice, but rather appear to be strongly pinned into a random configuration. The image in fig. 1*a*) was taken first at 4.2 K. Then the temperature was increased in steps. The highest temperature reached was 25 K (recall $T_c(R = 0) = 28$ K) where it was held for a few hours during other image acquisition. The temperature was then decreased in steps and the image in fig. 1*b*) was taken at 14 K. Note that we observe a change in relative vortex position even after this moderate temperature rise. We have not observed any vortex reorganization at 4.2 K.

The amplitude and size of the vortex field profile can be directly related to a physically significant quantity, the penetration depth λ. These profiles are temperature dependent. To extract $\lambda(T)$, we fit the images to a model calculation. We can model the system as a slab of superconductor with thickness d surrounded by vacuum. Since the magnetic penetration depth $\lambda \gg \xi$, the coherence length, in high-temperature superconductors, we may use the

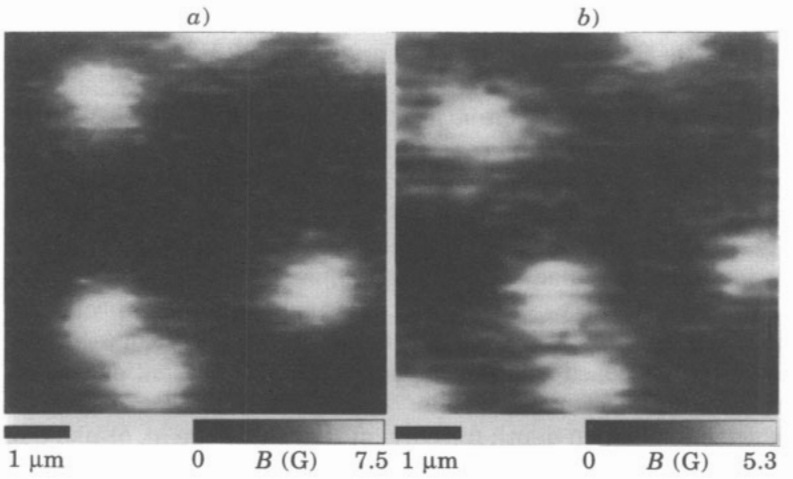

Fig. 1.

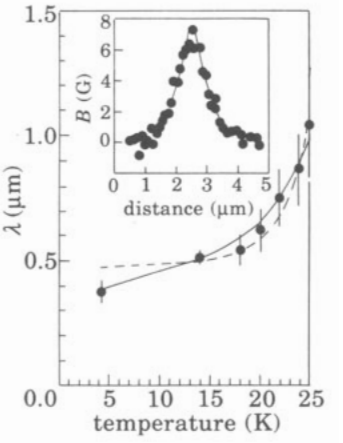

Fig. 2.

Fig. 1. – Magnetic-field images of the (001) sample taken 0.25 μm above the superconductor surface. Both images are $(5.85\,\mu m)^2$ in size. *a*) An image at 4.2 K showing several distinct vortices. *b*) The area at 14 K after an intermediate temperature rise up to 25 K. The shift between *a*) and *b*) is due to the temperature change.

Fig. 2. – Magnetic-field penetration depth λ resulting from fits to several images at different temperatures is shown as a function of temperature. It is compared to the two-fluid model $\lambda(T) = 4742/\sqrt{1-(T/26.3)^4}$ Å (– – –) and a three-parameter fit $\lambda(T) = 3500/\sqrt{1-(T/29.0)^{0.91}}$ Å (——), where the numerical values result from least-square fits. Inset: the vertical cross-section of the vortex in the lower right-hand quadrant of fig. 1*a*) is compared with the corresponding line of a 2-d fit. The fit yielded $\lambda = 3187$ Å for this vortex.

London equations to describe the fields within the superconductor. Laplace's equation applies *in vacuo*. If we assume the vortices pass through the superconductor straight along the normal, as would be the case if the superconductor were isotropic, the system has cylindrical symmetry. Following Pearl [16], we separate variables and expand the f's in Hankel components, and find that in the vacuum above the superconductor

$$B_z(r, z, \lambda) = \frac{\Phi_0}{2\pi\lambda^2}\int_0^\infty \mathrm{d}\gamma \frac{J_0(\gamma r)\exp[-\gamma(|z| - d/2)]}{k_\gamma(\mathrm{ctgh}\,(k_\gamma d/2) + k_\gamma/\gamma)}$$

with $k_\gamma = \sqrt{\gamma^2 + 1/\lambda^2}$. The integral is computed numerically. For distances greater than a few λ from the point where the flux emerges from the surface, the magnetic-field distribution resembles that of a magnetic monopole situated a distance $\sim\lambda$ below the surface. The physical size of the Hall bar is taken into account by convoluting the model field map with a rectangle equal to the size of the Hall bar.

We deduce λ by fitting the measured z-component magnetic-field images to the theoretical model. A least-squares routine varies the penetration depth, the vortex xy-positions, and a zero-field offset for the image. The height above the sample, the Hall-bar field calibration and the film thickness are known from other measurements. A slice from such a fit is shown along with a slice of the data in fig. 2 (inset). These cuts were taken from a fit of the image in fig. 1*a*) vertically through the vortex in the lower right quadrant. The averaged data collected from most vortices in a series of images at different temperatures is shown in fig. 2. The empirical

two-fluid model relation $\lambda(T) = \lambda(0)/\sqrt{1-(T/T_c)^4}$ for which T_c and $\lambda(0)$ were adjusted by a least-squares fit is shown in the figure as a dotted line. The three-parameter fit given by the solid line results when T_c, $\lambda(0)$ and the exponent of T/T_c are all varied by the least-squares routine. While the value of $\lambda(0) = 3500$ Å is somewhat larger than that (2185 Å) deduced from the best bulk materials ($T_c = 39$ K) via μSR [17], it is consistent with that of a bulk sample for which the Sr doping has been changed to reduce T_c to 28 K. In our thin films, a 5 K reduction in T_c arises from stresses due to a particularly large (-3.3%) lattice mismatch with the substrate for the (001) films [14, 15]. The additional T_c reduction ~ 5 K may result from slight nonoptimal growth conditions for this particular sample. The slope of the $\lambda(T)$ data at low temperatures is greater than the slope of the two-fluid model. This anomaly is also present in other data for the $La_{2-x}Sr_xCuO_4$ system [17]. Electronic inhomogeneities or thermal fluctuations of the vortices have been proposed as likely explanations. The present data show that the property persists at a local (few vortices) scale.

The $\lambda(T)$ discussed above is the penetration depth for current flowing in the (a, b)-plane of the $La_{1.85}Sr_{0.15}CuO_4$ superconductor. The behavior for current flowing in the c-direction is quite different, due to the anisotropic nature of the high-temperature superconductors. We investigate this anisotropy with the (103) film. The image shown in fig. 3 was taken 0.25 μm above the surface after cooling to 4.2 K in a 0.5 G field oriented perpendicular to the surface. In contrast to fig. 1, these vortices are elongated in the direction parallel to the (tilted) (a, b)-planes, which lie approximately 60° from the horizontal in the figure. The elongation is consistent with a longer λ for current flowing with a component in the c-direction. This extended λ along one axis of the vortex also reduces its maximum field. We measure ~ 0.5 G compared to ~ 7 G for the c-axis normal (001) film. Each vortex still contains one flux quantum for which $\sim 60\%$ of Φ_0 is accounted in a 10 μm^2 area (bright region in upper left of fig. 3). A quantitative analysis to deduce the λ anisotropy is complicated due to the lack of symmetry since the surface does not lie in any principal direction of the superconductor. Instead, we note that the magnitude at the center scales roughly as $1/[(z + \lambda_{ab}^{\text{eff}})(z + \lambda_c^{\text{eff}})]$ for

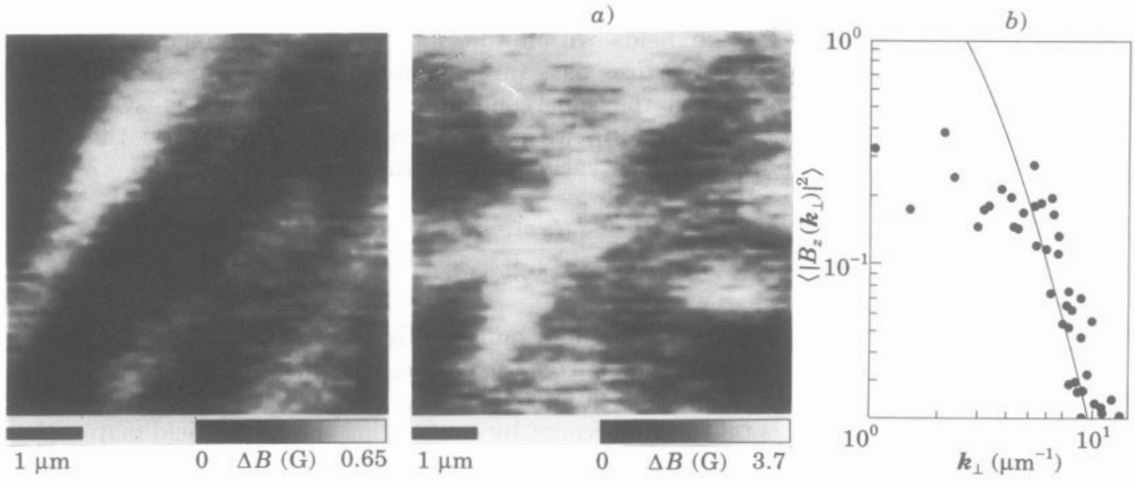

Fig. 3. Fig. 4.

Fig. 3. – Magnetic-field image of the (103) sample taken 0.25 μm above the superconductor surface at 4.2 K. The image is (5 μm)^2 in size.

Fig. 4. – *a*) Magnetic-field image 0.25 μm above a (001) sample at 4.2 K while a 1500 G field is applied. The image is (5.85 μm)^2. *b*) The measured $\langle |B_z(\boldsymbol{k}_\perp)|^2 \rangle$ from the image in *a*) (points) is compared with a theoretical calculation described in the text.

the (103) film compared to $1/(z + \lambda_{ab}^{\text{eff}})^2$ for the (001) film, where «effective» means that we must account for the effects of the film thickness [13]: $\lambda^{\text{eff}} = \lambda \operatorname{ctgh}(d/2\lambda)$. Using $\lambda_{ab} = 3500$ Å as found above, we obtain a value between 4 and 6 for the ratio λ_c/λ_{ab}.

While the effects of pinning are evident in the low-field data of fig. 1, we can investigate pinning quantitatively by imaging at much higher fields. An example of an image taken 0.25 μm above a sample cooled in a 1500 G field is shown in fig. 4*a*). We are no longer able to resolve individual vortices as the large λ allows the fields from neighboring vortices to overlap. Fluctuations of $B_z(\boldsymbol{r})$ in the image indicate variations in the local vortex density. The average square of a Fourier transform of these fluctuations $\langle |B_z(\boldsymbol{k}_\perp)|^2 \rangle$ yields the power density and is shown as a function of spatial frequency in fig. 4*b*). This has been deconvolved with the response function expected for a point source on the surface to make the data reflect surface field fluctuations.

The lattice deformations result from a competition between pinning forces and the elasticity of the vortex lattice. From anisotropic London theory, the linear elastic matrix $\Phi_{\alpha\beta}(\boldsymbol{k})$ of the flux line lattice (FLL) in anisotropic superconductors may be calculated [18]. This takes account of the long-range nature of the vortex-vortex interaction, which leads to an intrinsic softening of the FLL in hard type-II superconductors, and is therefore essential to its collective pinning [19] by dense randomly distributed weak-pinning centers. We obtain for the mean-square fluctuations of the z-component of the magnetic induction

$$\langle |B_z(\boldsymbol{k}_\perp)|^2 \rangle = \int_0^\infty \mathrm{d}k_z \, \frac{WB^2}{(1 + \lambda_{ab}^2 k^2)^2} \, \frac{k_\perp^2}{(c_{66} k_\perp^2 + c_{44}(\boldsymbol{k}) k_z^2)^2} ,$$

where the shear c_{66} and tilt c_{44} moduli are given by

$$c_{66} = \frac{B_c^2}{4\pi} \frac{1}{8\kappa^2} \frac{B}{B_c} \quad \text{and} \quad c_{44}(\boldsymbol{k}) = \frac{B^2}{4\pi} \frac{1}{1 + \lambda_c^2 k_\perp^2 + \lambda_{ab}^2 k_z^2} .$$

$W = n_p \langle f_p^2 \rangle$ gives the average strength of point pins of density n_p with individual strength f_p. We compute the above expressions analytically without approximations, and use W as a fitting parameter to obtain the amplitude of $\langle |B_z(\boldsymbol{k}_\perp)|^2 \rangle$, while λ_{ab} which determines the dispersion is set to 3500 Å. We use a value of 4 for the ratio $\lambda_c/\lambda_{ab} = \sqrt{M_z/M}$, 175 for κ and 45 T for the upper critical field B_c. We obtain values of $W = 5000$ and $7000\,\mathrm{erg^2/cm^5}$ for $B = 500$ and 1500 G, respectively. Note that the smaller (by 30%) observed field fluctuations, as the lattice becomes significantly stiffer at higher fields, result in a modestly larger W. These values of W are 2-3 orders of magnitude larger than that determined for bulk $Bi_2Sr_2CaCu_2O_8$ samples [20], which is reasonable considering the stronger pinning and shorter flux lattice correlation lengths that might be expected for the more defect-rich thin films. The strong vortex-vortex interaction within the film found at higher fields is important for the validity of this bulk calculation for a thin-film sample. At low fields, the long-range monopole surface interactions and possibly surface pinning become significant relative to the bulk intervortex interactions. A comparison of this calculation to the data at 1500 G is shown in fig. 4*b*) as a solid line. The limited range of model applicability in this system results in a factor of 2-3 uncertainty in our determination of W. The model does not describe fluctuations on a length scale larger than the translational elastic correlation length. This could be the source of the deviation at small $\boldsymbol{k}_\perp$ in fig. 4*b*). Indeed a correlation length $R_c \sim 0.8\,\mu\mathrm{m} = 6.5a$, where a is the FLL constant, is obtained at 1500 G from measured values of j_c and W, and the relation $Bj_c = \sqrt{W/V_c}$ for the correlated volume V_c. An independent estimate of R_c may be obtained from the Larkin length, above which the elasticity theory is not applicable, via [19]:

$R_c = c_{66}\, a/\sqrt{W}$ for a thin film. At 1500 G we obtain $R_c = 2.6a$, which agrees surprisingly well with the estimate obtained from the critical current. While this bulk collective pinning model is not expected to fully describe the thin film, it nevertheless does serve as a useful reference point from which the results can be understood.

In conclusion, we have developed a scanning Hall-probe microscope with submicron resolution, and demonstrated the imaging of individual vortices in $La_{1.85}Sr_{0.15}CuO_4$ films in both the isotropic (c-axis normal) and anisotropic (c-axis tilted) limits. The temperature-dependent local penetration depths extracted from individual vortices are consistent with penetration depths obtained with other techniques. Vortex density fluctuations can be used to estimate the pinning strength in a collective pinning model.

* * *

We gratefully acknowledge discussions with and assistance of J. VAN DER ZIEL, D. HARSHMAN, E. H. BRANDT and T. PALSTRA.

REFERENCES

[1] COFFEY H. T., *Cryogenics*, **7** (1965) 73; GOREN R. N. and TINKHAM M., *J. Low Temp. Phys.*, **5** (1971) 465.
[2] ITZLER M. A., SIMMONS J. A. and CHAIKIN P. M., *Bull. Am. Phys. Soc.*, **36** (1991) 724.
[3] AEPPLI G. *et al.*, *Phys. Rev. B*, **35** (1987) 7129.
[4] PINCAS P. *et al.*, *Phys. Lett.*, **13** (1964) 21.
[5] CRIBER D. *et al.*, *Phys. Lett.*, **9** (1964) 106.
[6] FORGAN E. M. *et al.*, *Nature*, **343** (1990) 735.
[7] NELSON D. R., *Phys. Rev. Lett.*, **60** (1988) 1973; BRANDT E. H., *Phys. Rev. Lett.*, **63** (1989) 1106; FISHER M. P. A., *Phys. Rev. Lett.*, **62** (1989) 1415.
[8] TRAEUBLE H. and ESSMANN U., *J. Appl. Phys.*, **25** (1968) 273.
[9] DOLAN G. V. *et al.*, *Phys. Rev. Lett.*, **62** (1989) 2184.
[10] MATSUDA T. *et al.*, *Phys. Rev. Lett.*, **66** (1991) 457.
[11] RICE P. and MORELAND J., *IEEE Trans. Magn.*, **27** (1991) 5181.
[12] OWUSU-SEKYERE K., CHANG A. M. and CHANG T. Y., *Appl. Phys. Lett.*, **52** (1988) 1246.
[13] CHANG A. M., HALLEN H. D., HESS H. F., KAO H. L., KWO J., WOLF R. and VAN DER ZIEL J., *Appl. Phys. Lett.*, **61** (1992) 1974.
[14] KAO H. L. *et al.*, *Appl. Phys. Lett.*, **59** (1991) 2748; KAO H. L., KWO J., FLEMING R. M., TAKAGI H. and HONG M., unpublished.
[15] KWO J., FLEMING R. M., KAO H. L., WERDEN D. J. and CHEN C. H., *Appl. Phys. Lett.*, **60** (1992) 1905.
[16] PEARL J., *J. Appl. Phys.*, **37** (1966) 4139.
[17] HARSHMAN D. R. and MILLS A. P. jr., *Phys. Rev. B*, **45** (1992) 10684.
[18] SUDBØ A. and BRANDT E. H., *Phys. Rev. Lett.*, **66** (1991) 1781.
[19] LARKIN A. I. and OVCHINNIKOV YU. N., *J. Low Temp. Phys.*, **34** (1979) 409.
[20] HOUGHTON A., PELCOVITS R. A. and SUDBØ A., *J. Phys. Condens. Matter*, **3** (1991) 7527.